Electromechanical Computing at 500°C with Silicon Carbide

Te-Hao Lee, *et al.*

Science **329**, 1316 (2010);
DOI: 10.1126/science.1192511

17. A. Cavalli, X. Salvatella, C. M. Dobson, M. Vendruscolo, *Proc. Natl. Acad. Sci. U.S.A.* **104**, 9615 (2007).
18. Y. Shen *et al.*, *Proc. Natl. Acad. Sci. U.S.A.* **105**, 4685 (2008).
19. D. S. Wishart *et al.*, *Nucleic Acids Res.* **36** (Web server issue), W496 (2008).
20. M. Allen, A. Friedler, O. Schon, M. Bycroft, *J. Mol. Biol.* **323**, 411 (2002).
21. P. Jemth *et al.*, *Proc. Natl. Acad. Sci. U.S.A.* **101**, 6450 (2004).
22. P. Jemth *et al.*, *J. Mol. Biol.* **350**, 363 (2005).
23. P. Jemth, C. M. Johnson, S. Gianni, A. R. Fersht, *Protein Eng. Des. Sel.* **21**, 207 (2008).
24. A. Matouschek, J. T. Kellis Jr., L. Serrano, A. R. Fersht, *Nature* **340**, 122 (1989).
25. J. P. Loria, M. Rance, A. G. Palmer III, *J. Am. Chem. Soc.* **121**, 2331 (1999).
26. D. F. Hansen, P. Vallurupalli, L. E. Kay, *J. Phys. Chem. B* **112**, 5898 (2008).
27. R. Ishima, D. A. Torchia, *J. Biomol. NMR* **25**, 243 (2003).
28. R. Ishima, J. Baber, J. M. Louis, D. A. Torchia, *J. Biomol. NMR* **29**, 187 (2004).
29. P. Lundström, D. F. Hansen, P. Vallurupalli, L. E. Kay, *J. Am. Chem. Soc.* **131**, 1915 (2009).
30. P. Lundström, D. F. Hansen, L. E. Kay, *J. Biomol. NMR* **42**, 35 (2008).
31. Single-letter abbreviations for the amino acid residues are as follows: A, Ala; C, Cys; D, Asp; E, Glu; F, Phe; G, Gly; H, His; I, Ile; K, Lys; L, Leu; M, Met; N, Asn; P, Pro; Q, Gln; R, Arg; S, Ser; T, Thr; V, Val; W, Trp; and Y, Tyr.
32. Materials and methods are available as supporting material on *Science* Online.
33. N. R. Skrynnikov, F. W. Dahlquist, L. E. Kay, *J. Am. Chem. Soc.* **124**, 12352 (2002).
34. N. Tjandra, A. Bax, *Science* **278**, 1111 (1997).
35. D. S. Wishart, D. A. Case, *Methods Enzymol.* **338**, 3 (2001).
36. M. V. Berjanskii, D. S. Wishart, *J. Am. Chem. Soc.* **127**, 14970 (2005).
37. Y. Shen, F. Delaglio, G. Cornilescu, A. Bax, *J. Biomol. NMR* **44**, 213 (2009).
38. S. Raman *et al.*, *Science* **327**, 1014 (2010); published online 4 February 2010 (10.1126/science.1183649).
39. R. Das, D. Baker, *Annu. Rev. Biochem.* **77**, 363 (2008).
40. M. Rückert, G. Otting, *J. Am. Chem. Soc.* **122**, 7793 (2000).
41. A. Fersht, *Structure and Mechanism in Protein Science: A Guide to Enzyme Catalysis and Protein Folding* (W. H. Freeman, New York, 1999).
42. T. L. Religa *et al.*, *Proc. Natl. Acad. Sci. U.S.A.* **104**, 9272 (2007).
43. A. Bax, *Curr. Opin. Struct. Biol.* **4**, 738 (1994).
44. M. Sattler, J. Schleucher, C. Griesinger, *Prog. Nucl. Magn. Reson. Spectrosc.* **34**, 93 (1999).
45. H. Q. Feng, Z. Zhou, Y. W. Bai, *Proc. Natl. Acad. Sci. U.S.A.* **102**, 5026 (2005).
46. B. G. Wensley *et al.*, *Nature* **463**, 685 (2010).
47. M. E. McCully, D. A. C. Beck, A. R. Fersht, V. Daggett, *Biophys. J.* **99**, 1 (2010).
48. S. W. Englander, L. Mayne, M. M. G. Krishna, *Q. Rev. Biophys.* **40**, 287 (2007).
49. P. Lundström *et al.*, *J. Biomol. NMR* **38**, 199 (2007).
50. V. Y. Orekhov, D. M. Korzhnev, L. E. Kay, *J. Am. Chem. Soc.* **126**, 1886 (2004).
51. Y. Shen, A. Bax, *J. Biomol. NMR* **38**, 289 (2007).
52. We thank J. Forman-Kay (Hospital for Sick Children, Toronto) for providing laboratory space and useful discussions, P. Jemth (Uppsala Univ.) for providing plasmids for protein expression, R. Vernon (Univ. of Washington, Seattle) for valuable discussions, and R. Muhandiram (Univ. of Toronto) for NMR support. T.L.R. acknowledges the European Molecular Biology Organization (ALTF 827-2006) and the Canadian Institutes of Health Research (CIHR) for postdoctoral fellowships. L.E.K. holds a Canada Research Chair in Biochemistry. This work was supported by a grant from the CIHR to L.E.K. The structural ensembles of the WT FF domain–folding intermediate have been deposited in the Protein Data Bank (PDB; www.rcsb.org) with accession code 2KZG.

Supporting Online Material
www.sciencemag.org/cgi/content/full/329/5997/1312/DC1
Materials and Methods
Figs. S1 and S2
Tables S1 to S4
References

3 May 2010; accepted 24 June 2010
10.1126/science.1191723

REPORTS

Electromechanical Computing at 500°C with Silicon Carbide

Te-Hao Lee,[1]* Swarup Bhunia,[2]* Mehran Mehregany[2]*

Logic circuits capable of operating at high temperatures can alleviate expensive heat-sinking and thermal-management requirements of modern electronics and are enabling for advanced propulsion systems. Replacing existing complementary metal-oxide semiconductor field-effect transistors with silicon carbide (SiC) nanoelectromechanical system (NEMS) switches is a promising approach for low-power, high-performance logic operation at temperatures higher than 300°C, beyond the capability of conventional silicon technology. These switches are capable of achieving virtually zero off-state current, microwave operating frequencies, radiation hardness, and nanoscale dimensions. Here, we report a microfabricated electromechanical inverter with SiC complementary NEMS switches capable of operating at 500°C with ultralow leakage current.

High-temperature measurement and control instrumentation require microcontrollers, in addition to sensors and interface electronics, for a variety of important applications (such as automotive and aerospace propulsion systems, deep-well drilling, and geothermal exploration) in which the ambient temperature typically ranges from 300° to 600°C (*1*). However, limited by their band gaps, the mature silicon technologies [for example, a complementary metal-oxide semiconductor (CMOS)] are not applicable to this field due to excessive leakage caused by p-n junction degradation and thermoionic leakage (*2*). At these temperatures, thermally excited electrons in silicon can overcome the gate potential, and the intrinsic carriers excited by the thermal energy exceeds the amount of doped carriers. Thus, the electrical properties will be considerably influenced by thermally generated carriers, and the devices fail. To this end, wide–band-gap semiconductors like SiC have been of interest for these applications. Such materials, with adequate conductivity, offer a potential solution to expensive thermal-management and heat-sinking requirements, which pose a major barrier to continued shrinking of electronics. To date, the SiC electronic platform has been regarded as the most viable technology for high-temperature applications. Various field-effect transistor (FET) architectures have been considered as building blocks of this platform. Among alternative device architectures, the SiC junction field-effect transistor (JFET) is the most promising candidate for high-temperature logic applications (*3*, *4*). Lack of good-quality gate insulator and low inversion-layer mobility have limited the development of SiC metal-oxide semiconductor FETs (*5*–*7*). On the other hand, Shottky-based metal semiconductor FETs exhibit notable gate-to-channel leakage at elevated temperatures (*8*). As a depletion-mode device, the JFET

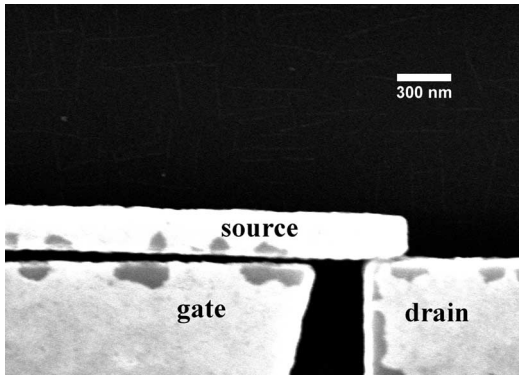

Fig. 1. A scanning electron micrograph showing the ON state of the three-terminal SiC NEMS switch. The spacing between the gate and drain is 300 nm. The initial actuation-gap height, defined as the distance between source and gate, is 150 nm without applying any potential. Lateral movement of the cantilever due to electrostatic attraction between the source and gate causes the beam to contact the drain. After the contact of source and drain, the gap between source and gate becomes only 25 nm.

[1]Department of Materials Science and Engineering, Case Western Reserve University, Cleveland, OH 44106, USA. [2]Department of Electrical Engineering and Computer Science, Case Western Reserve University, Cleveland, OH 44106, USA.
*To whom correspondence should be addressed. E-mail: tehao@case.edu (T.-H.L.); swarup.bhunia@case.edu (S.B.); mehran@case.edu (M.M.)

alleviates these problems. However, the large-size, high-threshold voltage, and low switching speed makes logic design with SiC JFETs unattractive. In addition, the wasted power caused by leakage current increases markedly with rising temperature. Replacing existing SiC JFETs with nanoelectromechanical system (NEMS) switches is an attractive alternative for low-power, high-performance logic operation (*9*–*11*) at high temperatures. These switches can achieve virtually zero off-state current (that is, almost no leakage current), can be fabricated at nanoscale dimensions, and can operate at microwave frequencies (up to 1 GHz) (*12*–*14*). The excellent thermal stability, chemical inertness, and mechanical robustness make SiC a suitable material for this technology. High-temperature packaging is usually a challenge (*15*); it is accomplished with the use of ceramic (e.g., Al_2O_3 and AlN) packages incorporating gold-wire bonding (*16*, *17*). For example, high-temperature packaging for a SiC pressure sensor has been demonstrated by Chen and Mehregany for in-cylinder pressure monitoring (*18*). In addition, thousands of operation hours of SiC JFETs at 500°C using Al_2O_3 package substrate and gold bonding wire has been demonstrated by Neudeck *et al.* (*3*). Here, we report the microfabrication of an electromechanical inverter using SiC complementary NEMS switches that operates at 500°C with ultralow leakage current (four orders of magnitude less than SiC JFETs). This logic element, which is also radiation tolerant, presents a technology basis for all-mechanical computation at high operational temperatures.

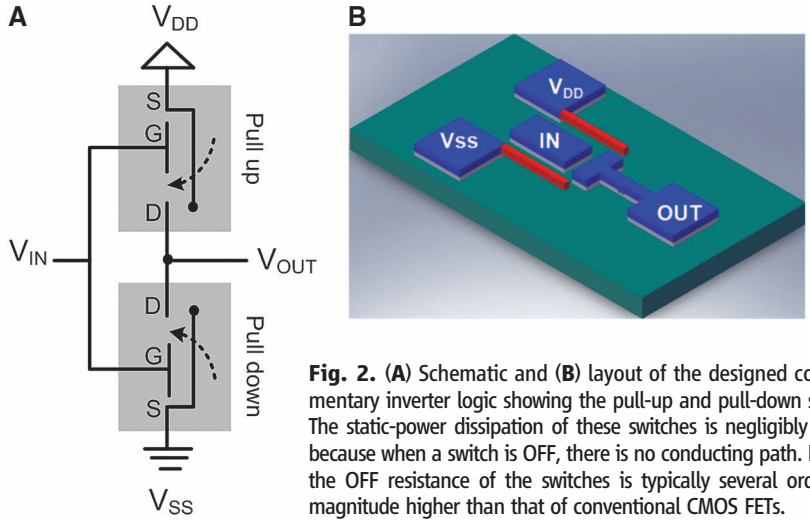

Fig. 2. (**A**) Schematic and (**B**) layout of the designed complementary inverter logic showing the pull-up and pull-down stages. The static-power dissipation of these switches is negligibly small, because when a switch is OFF, there is no conducting path. Hence, the OFF resistance of the switches is typically several orders of magnitude higher than that of conventional CMOS FETs.

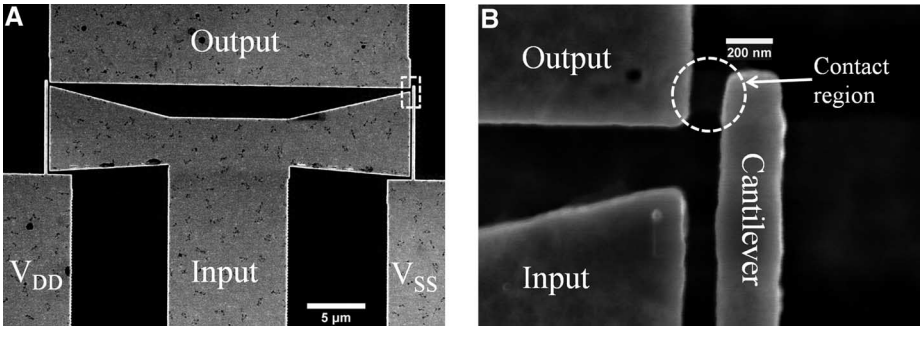

Fig. 3. Scanning electron micrographs of (**A**) a fabricated inverter with (**B**) a magnified picture highlighted in (A) showing the cantilever connected to V_{SS} and the corresponding actuation gap.

Fig. 4. Input-output voltage waveform of the inverter at 500°C. The output voltage maintains inverting behavior, although the voltage swing shows slight degradation.

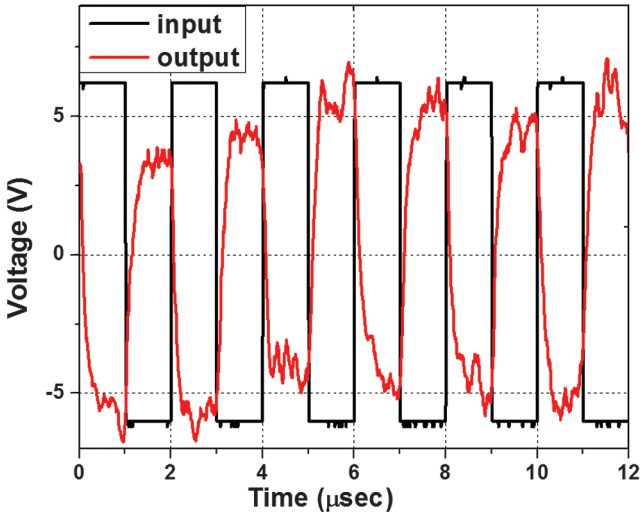

The electromechanical inverter is designed using two laterally actuated NEMS switches following a complementary static-CMOS logic style (*19*), which consists of pull-up and pull-down stages. Each switch has three terminals: source (S), gate (G), and drain (D), where the gate is used as a control terminal to create a conducting path between the drain and source through electrostatic actuation. As shown in Fig. 1, the ON state of the switch is represented by the contact of the S and D to form the conducting "channel." Figure 2A shows the schematic of the inverter. This logic style was chosen because it provides low noise sensitivity and low static-power consumption.

The fabricated SiC inverters (Fig. 3) consist of two identical three-terminal switches; the length, width, and actuation gap of the cantilevers are ~8, ~200, and 150 nm, respectively. A 100-mm-diameter (100) Si wafer with a 500-nm-thick thermally grown silicon dioxide layer is used as the substrate. Heavily nitrogen-doped ($N_D \sim 1 \times 10^{20}$ cm^{-3}) polycrystalline 3C-SiC films are deposited on the wafer by low-pressure chemical-vapor deposition to a thickness of 400 nm (*20*). Next, a 40-nm-thick Ni etching mask layer is deposited by thermal evaporation and patterned by electron-beam lithography and lift-off. The Ni etch mask pattern is then transferred to the SiC film by deep reactive-ion etching with SF_6 as etch gas. HF wet etching removes the sacrificial silicon dioxide layer, followed by carbon dioxide critical point drying to suspend the patterned SiC beams above the Si substrate.

The two laterally actuated cantilevers of the inverter are connected to positive- (V_{DD}) and negative-voltage (V_{SS}) terminals, respectively. When applying a positive input (logic high), the electrostatic force between the input and the cantilever connected to V_{SS} overcomes the restoring force of the beam, and the cantilever moves laterally to contact the output, providing a logic low. A logic high can be obtained by supplying a negative input to actuate the beam connected to V_{DD}. Due to the complementary nature of the logic, the output terminal (V_{OUT}) is connected to either V_{DD} (for logic "0" at the input terminal V_{IN}) or V_{SS} (for logic "1" at V_{IN}), but not both, thus preventing any direct current path at the steady state. Switches have been verified to work at 500°C in air. However, to prevent surface oxidation, we conducted high-temperature testing in a nitrogen environment

using a resistive heater, with the devices packaged in ceramic dips. Field applications would make use of a vacuum package, which also prevents surface oxidation and additionally eliminates viscous drag forces during switch operation.

Inverter operation has been demonstrated at 500°C (Fig. 4) with $V_{DD} = 6$ V and $V_{SS} = -6$ V, at an operating speed of 500 kHz. The logic level is clearly higher than the existing Si logic devices, which operate at 3 V or lower. However, the threshold voltage of the fabricated switches is compatible to other competing high-temperature electronics (*3*, *4*). The logic level can be further reduced by narrowing the actuation gap (*21*) as the nanofabrication technology advances. NEMS switches based on carbon nanotubes exhibiting a threshold voltage smaller than 4 V have been demonstrated with gaps smaller than 100 nm (*22*, *23*). In theory, the actuation voltage of the NEMS switches can be scaled beyond the threshold voltage of CMOS, whose scaling is limited by the thermal voltage k_BT/q (here, k_B is the Boltzmann constant, T is temperature, and q is the charge of an electron). The active area of the demonstrated inverter consisting of two complementary NEMS switches is ~8 μm^2, excluding connecting traces and contact pads. Compared to modern (90-nm gate length) nanoscale Si CMOS logic devices, which have a standard-cell inverter gate with a minimum active area of ~0.1 μm^2 (*24*), the presented device is much larger. However, this demonstrated inverter is already about three orders of magnitude smaller than most reported high–temperature, JFET-based logic gates, which have gate lengths ranging from tens to few hundreds of microns (*3*, *4*). With improvement in nanolithography, it appears very plausible to scale the dimensions of the NEMS switches to achieve higher integration density, along with lower operating voltage and higher switching speed.

Typical switches have operated ≥21 billion cycles at 25°C and ≥2 billion cycles at 500°C; the measured leakage current at the OFF state is less than 10 fA (below the noise floor of the measuring tool). Failure at 25°C is breakage of the switching cantilever beam at the location of highest stress, characterized by a clean fracture. However, at 500°C, the broken cantilever beam has a ball of SiC at one side of the fracture gap that is likely to be local melting—an unexpected event because SiC sublimates at 1800°C. Thus, the mechanism for the high-temperature failure is not yet understood. Overall, this achievement of a SiC NEMS-based inverter operating at 500°C creates a pathway toward energy-efficient high-temperature computation.

References and Notes

1. P. G. Neudeck, R. S. Okojie, L.-Y. Chen, *Proc. IEEE* **90**, 1065 (2002).
2. J. Goetz, *Sensors Mag.* **17**, 20 (2000).
3. P. G. Neudeck *et al.*, *IEEE Electron Device Lett.* **29**, 456 (2008).
4. A. C. Patil, X.-A. Fu, C. Anupongongarch, M. Mehregany, S. L. Garverick, *J. Microelectromech. Syst.* **18**, 950 (2009).
5. J. W. Palmour *et al.*, *Diamond Related Mater.* **6**, 1400 (1997).
6. S. Potbhare, N. Goldsman, G. Pennington, A. Lelis, J. M. McGarrity, *J. Appl. Phys.* **100**, 044515 (2006).
7. F. Moscatelli, A. Poggi, S. Solmi, R. Nipoti, *IEEE Trans. Electron. Dev.* **55**, 961 (2008).
8. J. W. Palmour, J. A. Edmond, H. S. Kong, C. H. Carter Jr., *Physica B* **185**, 461 (1993).
9. M. Y. A. Yousif, P. Lundgren, F. Ghavanini, P. Enoksson, S. Bengtsson, *Nanotechnology* **19**, 285204 (2008).
10. T. Rueckes *et al.*, *Science* **289**, 94 (2000).
11. K. Akarvardar, H.-S. P. Wong, *IEEE Electron Device Lett.* **30**, 626 (2009).
12. X. L. Feng, C. J. White, A. Hajimiri, M. L. Roukes, *Nat. Nanotechnol.* **3**, 342 (2008).
13. A. K. Naik, M. S. Hanay, W. K. Hiebert, X. L. Feng, M. L. Roukes, *Nat. Nanotechnol.* **4**, 445 (2009).
14. X. M. H. Huang, C. A. Zorman, M. Mehregany, M. L. Roukes, *Nature* **421**, 496 (2003).
15. E. Savrun, *Sensors 2002. Proc. IEEE* **2**, 1139 (2002).
16. K. Meyyappan, P. McCluskey, L. Chen, *IEEE Trans. Device Mater. Reliab.* **3**, 152 (2003).
17. L.-Y. Chen, R. S. Okojie, P. G. Neudeck, G. W. Hunter, S.-T. T. Lin, *Mater. Res. Soc. Symp. Proc.* **682E**, N.4.3.1 (2001).
18. L. Chen, M. Mehregany, *Sens. Actuators A Phys.* **145–146**, 2 (2008).
19. R. Zimmermann, W. Fichtner, *IEEE J. Solid-State Circuits* **32**, 1079 (1997).
20. Materials and methods are available as supporting material on *Science* Online.
21. K. Akarvardar *et al.*, *IEEE Trans. Electron. Dev.* **55**, 48 (2008).
22. A. B. Kaul, E. W. Wong, L. Epp, B. D. Hunt, *Nano Lett.* **6**, 942 (2006).
23. S. N. Cha *et al.*, *Appl. Phys. Lett.* **86**, 083105 (2005).
24. See IBM 90-nm standard-cell library from ARM.

25. This work was supported by the Defense Advanced Research Projects Agency Microsystem Technology Office NEMS program under grant N66001-07-1-2031.

Supporting Online Material

www.sciencemag.org/cgi/content/full/329/5997/1316/DC1
Materials and Methods
SOM Text
Fig. S1
Table S1
References

19 May 2010; accepted 23 July 2010
10.1126/science.1192511

A Red-Shifted Chlorophyll

Min Chen,[1]* Martin Schliep,[1] Robert D. Willows,[2] Zheng-Li Cai,[3] Brett A. Neilan,[4] Hugo Scheer[1,5]

Chlorophylls are essential for light-harvesting and energy transduction in photosynthesis. Four chemically distinct varieties have been known for the past 60 years. Here we report isolation of a fifth, which we designate chlorophyll f. Its in vitro absorption (706 nanometers) and fluorescence (722 nanometers) maxima are red-shifted compared to all other chlorophylls from oxygenic phototrophs. On the basis of the optical, mass, and nuclear magnetic resonance spectra, we propose that chlorophyll f is [2-formyl]-chlorophyll a ($C_{55}H_{70}O_6N_4Mg$). This finding suggests that oxygenic photosynthesis can be extended further into the infrared region and may open associated bioenergy applications.

Chlorophylls (Chls) are the essential pigments of photosynthesis, for which they both harvest light and transduce it into chemical energy. There are four chemically distinct chlorophylls known to date in oxygenic photosynthetic organisms, termed Chls a, b, c, and d in the order of their discovery (*1*, *2*). All four pigments are present in light-harvesting complexes, though until recently only Chl a was thought to be indispensable for energy transduction in the photosystem reaction centers (*3*). This paradigm was challenged when Chl d, long considered an artifact since its discovery in 1943 (*4*), was shown to constitute up to 99% of all Chl in the cyanobacterium *Acaryochloris marina* (*5*). In this and related organisms, Chl d can replace Chl a in the photosystems of oxygenic photosynthesis, thereby extending to the red the spectrum of light that can be harvested for carbon fixation (*6*). Here we report yet another chlorophyll, which we designate Chl f (*2*), that absorbs even further to the red.

The morphological features of stromatolites provide a unique environment for specific but diverse cyanobacterial communities (*7*). We cultured a sample from Hamelin pool under near-infrared light (720 nm) (*8*). Analysis of a methanolic extract of stromatolites from Shark Bay, Western Australia, by high-performance liquid chromatography (HPLC) revealed a complex mixture of chlorophylls (Fig. 1A): In addition to a detectable amount of Chl a (peak 3) and bacteriochlorophyll a (peak B), there were trace amounts of Chl d and a new pigment, Chl f (peak 2 in Fig. 1A). The optical absorption spectrum of Chl f in neat methanol has a red-shifted Q_Y transition [wavelength of maximum absorption (λ_{max}) = 706 nm] compared to other chlorophylls and a blue-shifted Soret band (λ_{max} = 406 nm) (Fig. 1, B and D). The room-temperature fluorescence emission of isolated Chl f is maximal at 722 nm (with excitation wavelength of 407 nm) (Fig. 1D), which is also considerably red-shifted compared to other Chls (*9*). Chlorophyll f appears to be made by a filamentous cyanobacterium (fig. S3) based on the 16*S* ribosomal RNA (rRNA) sequence of our purest enrichment III culture (see supporting text), which contained only Chl a and Chl f by HPLC analysis.

We assigned the molecular formula of Chl f ($C_{55}H_{70}O_6N_4Mg$) by mass spectral analysis based on the molecular ion at 906 *m/z* (mass/charge ratio). Phytol ($C_{20}H_{38}$) was identified by the prominent fragment at 628 *m/z* (fig. S1B), and Mg as the central metal by the molecular ion of the pheophytin (Pheo) (884 *m/z*, $C_{55}H_{72}O_6N_4$). A

[1]School of Biological Sciences, University of Sydney, NSW 2006, Australia. [2]Department of Chemistry and Biomolecular Sciences, Macquarie University, NSW 2109, Australia. [3]School of Chemistry, University of Sydney, NSW 2006, Australia. [4]School of Biotechnology and Biomolecular Science, University of New South Wales, NSW 2052, Australia. [5]Department of Biology I, University of Munich, D-80638 Muenchen, Germany.

*To whom correspondence should be addressed. E-mail: min.chen@sydney.edu.au